

# UMGAD: Unsupervised Multiplex Graph Anomaly Detection

Xiang Li<sup>1</sup>, Jianpeng Qi<sup>1</sup>, Zhongying Zhao<sup>2</sup>, Guanjie Zheng<sup>3</sup>, Lei Cao<sup>4</sup>, Junyu Dong<sup>1</sup>, Yanwei Yu<sup>1</sup>✉

<sup>1</sup>Faculty of Information Science and Engineering, Ocean University of China, Qingdao, China

<sup>2</sup>College of Computer Science and Engineering, Shandong University of Science and Technology, Qingdao, China

<sup>3</sup>Department of Computer Science and Engineering, Shanghai Jiao Tong University, Shanghai, China

<sup>4</sup>Department of Computer Science, The University of Arizona, Tucson, USA

lixiang1202@stu.ouc.edu.cn, zyzhao@sdust.edu.cn, gjzheng@sjtu.edu.cn, lcao@csail.mit.edu,  
 {qijianpeng, dongjunyu, yuyanwei}@ouc.edu.cn

**Abstract**—Graph anomaly detection (GAD) is a critical task in graph machine learning, with the primary objective of identifying anomalous nodes that deviate significantly from the majority. This task is widely applied in various real-world scenarios, including fraud detection and social network analysis. However, existing GAD methods still face two major challenges: (1) They are often limited to detecting anomalies in single-type interaction graphs and struggle with multiple interaction types in multiplex heterogeneous graphs. (2) In unsupervised scenarios, selecting appropriate anomaly score thresholds remains a significant challenge for accurate anomaly detection. To address the above challenges, we propose a novel Unsupervised Multiplex Graph Anomaly Detection method, named UMGAD. We first learn multi-relational correlations among nodes in multiplex heterogeneous graphs and capture anomaly information during node attribute and structure reconstruction through graph-masked autoencoder (GMAE). Then, to further extract abnormal information, we generate attribute-level and subgraph-level augmented-view graphs respectively, and perform attribute and structure reconstruction through GMAE. Finally, We learn to optimize node attributes and structural features through contrastive learning between original-view and augmented-view graphs to improve the model’s ability to capture anomalies. Meanwhile, we also propose a new anomaly score threshold selection strategy, which allows the model to be independent of ground truth information in real unsupervised scenarios. Extensive experiments on four datasets show that our UMGAD significantly outperforms state-of-the-art methods, achieving average improvements of 13.48% in AUC and 11.68% in Macro-F1 across all datasets. The source code of our model is available at <https://anonymous.4open.science/r/UMGAD-1F3B>.

**Index Terms**—graph anomaly detection, multiplex heterogeneous graph, graph-masked autoencoder

## I. INTRODUCTION

Anomaly detection [1]–[3], aimed at identifying entities that deviate significantly from normal conditions, is extensively utilized across various applications, for example, fraudulent user detection in financial networks [4]–[8], anomalous behavior detection in social networks [9]–[12], malicious comments in review networks [13], review-scrubbing buffs in e-commerce networks [14], [15], and so on. Unlike time series anomaly detection, GAD presents greater challenges due to the inherent complexity of graph data [16]–[19], which typically

encompasses node attributes and structural features [20]–[22]. This complexity renders the task of capturing anomalies within graphs particularly formidable.

Due to the high cost of acquiring real anomaly data, a large number of existing GAD methods are performed in an unsupervised manner [23]–[26], to detect instances that deviate significantly from the majority of data. Various methods have been proposed to solve the unsupervised graph anomaly detection (UGAD) problem. They can be broadly categorized into the following types: traditional methods, message passing-improved (MPI) methods, contrastive learning (CL)-based methods, graph autoencoder (GAE)-based methods, and Multi-view (MV) methods, etc. Early traditional UGAD methods such as [27] are usually based on machine learning algorithms to encode graph information and detect anomalies, or utilize residual information to capture anomalous features. Message passing-improved methods [28], [29] learn anomalous node features by improving the message-passing mechanism of GNNs. Recently, with the rapid development of graph neural networks (GNNs), more and more CL-based [30] and GAE-based methods have emerged. For example, GRADATE [31] performs anomaly detection through a multi-scale contrastive learning network with augmented views, and VGOD [32] combines variance-based and graph reconstruction-based models through contrastive learning to detect anomalies. ADAGAD [33] builds a denoised graph first to train the graph encoder and then trains the graph decoder on the original graph for reconstructing node attributes and structure.

**Challenges.** Existing UGAD approaches, such as CL-based and GAE-based methods, have achieved promising results. Nevertheless, the UGAD task still faces the following two major challenges: (1) *Most existing methods focus solely on non-multiplex heterogeneous graphs, while real-world graphs are often multiplex that typically include multiple types of interactions.* For example, there exists viewing, carting, and buying relations between users and items in e-commerce networks, or users’ different comments and rating scores on items in review networks. These interactions result in complex structures, known as multiplex heterogeneous graphs. Anomaly detection

in multiplex heterogeneous graphs is challenging because the interacting multiple relations are extremely complex and different types of relations have different effects on anomaly detection. (2) *In real unsupervised scenarios, most of existing aspects face difficulties in selecting anomaly score thresholds because the number of anomalies is unknown.* Existing models typically employ two approaches to select the anomaly score threshold: 1) by selecting the threshold based on the known number of anomalies when ground truth information in the test set is available, and 2) by choosing the threshold that yields the best model performance. However, these methods are not suitable when the number of anomalies and their labels are unknown, making it unreasonable to rely on these approaches for threshold selection in the real unsupervised scenario with no ground truth information from the test set.

**Presented Work.** Recognizing the above challenges, we focus on exploring the important impact of different interactive relations on node representation learning and extracting anomaly information through graph reconstructions for multiplex heterogeneous graphs. To this end, this paper proposes a novel unsupervised multiplex graph anomaly detection method, named UMGAD. We first learn multi-relational correlations among nodes in multiplex heterogeneous graphs and capture anomaly information during node attribute and structure reconstruction in the original-view graph. Then, to further extract abnormal information, we generate attribute-level and subgraph-level augmented-view graphs respectively, and perform attribute and structure reconstruction in the augmented-view graph. Innovatively, we coordinate the fusion of GMAEs with multiple masking mechanisms across multiplex graphs to reconstruct node attributes, network structures, and subgraphs in the original and augmented graphs. Furthermore, we learn to optimize node attributes and structural features through contrastive learning between original-view and augmented-view graphs to improve the model’s ability to capture anomalies. Meanwhile, we also propose a new anomaly score threshold selection strategy, which allows the model to be independent of the ground truth in real unsupervised scenarios. Extensive experiments on datasets with synthetic and real anomalies have demonstrated the effectiveness and efficiency of UMGAD compared with state-of-the-art UGAD methods.

This work makes the following contributions:

- We propose a novel unsupervised multiplex graph anomaly detection method named UMGAD that emphasizes the importance of constructing and exploiting different interactions between nodes and addresses the problem of unsupervised anomaly detection in multiplex heterogeneous graphs.
- We design an effective method for selecting appropriate anomaly score thresholds in the real unsupervised scenario without involving the ground truth by performing anomaly information extraction on both the original- and the augmented-view graphs.
- We conduct extensive experiments on datasets with both synthetic and real anomalies to demonstrate the superiority and efficiency of our proposed method. Experiment

results show that UMGAD achieves 13.48%, and 11.68% average improvement in terms of AUC and macro-F1 across four datasets compared to SOTA baselines.

## II. RELATED WORK

UGAD has attracted increasing attention in recent years, many researchers focus on how to use self-supervised signals to improve the model’s ability to detect anomalies in unsupervised scenarios. Early traditional UGAD methods, such as Radar [27] and ResGCN [34], which capture anomalous features by describing the residuals of attribute information and their consistency with network information, are concise and effective. With the rapid development of GNNs, it has also been naturally introduced into the field of anomaly detection, and recent researchers have been trying to develop UGAD models based on GNNs. We broadly categorize GNN-based models into four types: MPI methods, CL-based methods, GAE-based methods and MV methods.

**MPI methods.** It is well known that most of the GNN-based methods exploit the message passing mechanism [35] of GNN to learn node attributes by aggregating the neighborhood information of nodes. However, due to the feature inconsistency between normal and anomalous nodes, the original message passing mechanism may impair the model’s ability to extract the anomalous information. Luo et al. [28] enhance the message passing mechanism through community segmentation and structure learning, obtaining node attributes by introducing the community structure. Ber et al. [36] propose RAND, a reinforcement learning-based method for unsupervised graph anomaly detection, which enriches neighbor pools, evaluates reliability, selects the best subset, and amplifies messages from reliable neighbors. Qiao et al. [29] propose TAM, a truncated affinity maximization method that maximizes local affinity with neighbors and performs node characterization on a truncated graph instead of the original graph.

**CL-based methods.** As a common method for mining self-supervised signals [37]–[39], contrastive learning is also introduced to the UGAD task [40] to capture feature inconsistencies between normal and anomalous nodes. CoLA [41] introduces a contrastive instance pair sampling method that leverages local network information to embed high-dimensional attributes and local structures. Zhang et al. [42] propose Sub-CR, a self-supervised model combining multi-view contrastive learning and attribute reconstruction for anomaly detection on attribute networks. GRADATE [31] extends contrastive learning to the subgraph level with node-subgraph and subgraph-subgraph contrastive learning, effectively identifying complex structural anomalies. Huang et al. [32] integrate variance-based and attribute reconstruction models for balanced outlier detection.

**GAE-based methods.** GAE-based methods [43] are one of the mainstay methods to detect anomalies by reconstructing the node attributes and structural features in the graphs. Ding et al. [44] leverage GCN to model graph topology and node attributes for learning node embeddings. Roy et al. [45] propose GAD-NR, which reconstructs a node’s entire neighborhood based on its representation, encompassing

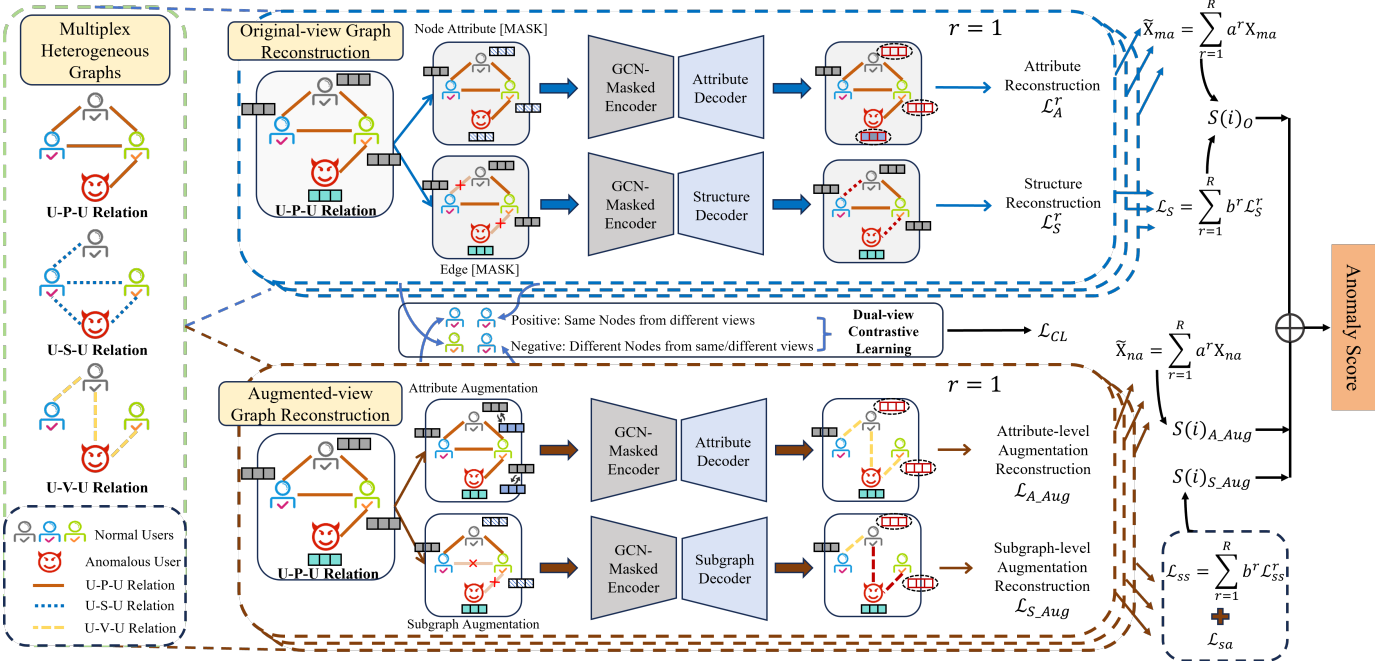


Fig. 1: The overview of the proposed UMGAD. There are three interaction types in the multiplex heterogeneous graph: U-P-U links users reviewing at least one product, U-S-U link users having at least one identical star rating within a week, U-V-U links linguistically similar users.

local structure, self-properties, and neighborhood properties. ADA-GAD [33] introduces a two-stage anomaly denoising autoencoder framework. The first stage trains the GAE on denoised graphs, while the second retrains the encoder on original graphs with anomaly distribution regularization to prevent overfitting.

**MV methods.** Additionally, some recent methods have focused on the GAD task on multiplex graphs, which we categorize as multi-view GAD methods. AnomMAN [46] detects anomalies on multi-view attribute networks by considering attributes and interactions across views, using an attention mechanism to fuse their importance. DualGAD [13] adopts a dual-bootstrapped self-supervised approach to tackle feature-structure inconsistency and imbalanced anomaly signals. It combines subgraph reconstruction with a cluster-guided contrastive learning mechanism, achieving state-of-the-art performance in node-level anomaly detection.

### III. PRELIMINARY

Generally, a network is denoted as  $\mathcal{G} = \{\mathcal{V}, \mathcal{E}, \mathcal{X}\}$ , where  $\mathcal{V}$  is the collection of nodes, and  $\mathcal{E}$  is the collection of edges between nodes, and  $\mathcal{X}$  is the collection of node attributes.

**Definition 1** (Multiplex Heterogeneous Graphs, MHGs). *Given the defined network  $\mathcal{G}$ , a multiplex heterogeneous graph can be divided into  $R$  relational subgraphs  $\mathcal{G} = \{\mathcal{G}^1, \mathcal{G}^2, \dots, \mathcal{G}^R\}$ , where  $R$  denotes the number of interactive relation categories. Each subgraph is defined as  $\mathcal{G}^r = \{\mathcal{V}, \mathcal{E}^r, \mathcal{X}\}$ , where  $\mathcal{V}$  and  $\mathcal{X} \in \mathbb{R}^{|\mathcal{V}| \times f}$  denote the set of all nodes and node attributes respectively,  $f$  is the size of the node attribute,  $\mathcal{E}^r$  represents the edge set in the  $r$ -th*

*relational subgraph,  $\mathcal{R} = \{1, 2, \dots, R\}$  represents the set of edge relation categories,  $|\mathcal{R}| = R$ , and  $\mathcal{E} = \bigcup_{r \in \mathcal{R}} \mathcal{E}^r$  is the collection edge set of various relation subgraphs.*

Next, we formally define our studied problem in this work.

**Problem** (Unsupervised Multiplex Graph Anomaly Detection, UMGAD). *Given a multiplex graph  $\mathcal{G}$ , the unsupervised GAD problem aims to identify nodes that significantly deviate from the majority in both structural features and node attributes. We try to define an anomaly function  $S(i)$  that assigns an anomaly score to each node  $v_i \in \mathcal{V}$ . Nodes with scores exceeding the selected anomaly threshold are classified as anomalous, while others are considered normal.*

## IV. METHODOLOGY

In this section, we propose a novel unsupervised multiplex graph anomaly detection method, named UMGAD, depicted in Fig. 1. It mainly includes three key components: (1) *Original-view Graph Reconstruction*, (2) *Augmented-view Graph Reconstruction* and (3) *Dual-view Contrastive Learning*.

### A. Original-view Graph Reconstruction

1) *Attribute Reconstruction*: Attribute inconsistency is one of the most important evidence to distinguish abnormal and normal nodes in the feature space. However, the aggregation mechanism of existing GNN models is based on the homogeneity assumption. It is detrimental to identifying rare abnormal nodes because most of the connected normal nodes will weaken the abnormal information during message propagation, thus smoothing the attribute inconsistency to hinder the abnormality detection, especially in MHGs. To learn the

importance of different relations for UGAD in MGHs, we first decouple the original graph into multiple relational subgraphs. Then we mask each relational subgraph with an attribute masking strategy. Formally, we get the subgraph  $\mathcal{G}^r$  and randomly sample a subset  $\mathcal{V}_{ma}$  with a masking ratio  $r_m$  and then obtain the perturbation subgraph as follows:

$$\mathcal{G}_{ma}^r = (\mathcal{V}, \mathcal{E}, \mathcal{X}_{ma}), \quad (1)$$

where the original node attributes in  $\mathcal{X}_{ma}$  are replaced by the [MASK] tokens which are learnable vectors. Masked nodes are selected by utilizing uniform random sampling without replacement, which helps prevent potential bias. We repeat the attribute masking strategy on each relational subgraph for  $K$  times to finally generate a set of masked subgraphs  $\mathcal{G}_{ma}^r = \{\mathcal{G}_{ma}^{r,1}, \mathcal{G}_{ma}^{r,2}, \dots, \mathcal{G}_{ma}^{r,K}\}$  for  $\mathcal{G}^r$ . These masked subgraphs are then fed into the GNN-based encoder and decoder and the output of each encoder is:

$$\mathcal{X}_{ma}^{r,k} = Dec(Enc(\mathcal{V}_{re}, \mathcal{E}^r | \mathbf{W}_{enc1}^{r,k}), \mathcal{E}^r | \mathbf{W}_{dec1}^{r,k}), \quad (2)$$

where  $\mathcal{X}_{ma}^{r,k} \in \mathbb{R}^{|\mathcal{V}| \times f}$  is the output of the attribute decoder in the  $k$ -th masking repeat of the  $r$ -th relational subgraph.  $\mathcal{V}_{re} = \mathcal{V} \setminus \mathcal{V}_{ma}$  denotes the set of remaining nodes that are unaffected by masking,  $\mathbf{W}_{enc1}^{r,k} \in \mathbb{R}^{f \times d_h}$  and  $\mathbf{W}_{dec1}^{r,k} \in \mathbb{R}^{d_h \times f}$  are the trainable weight matrices. Inside each encoder and decoder, before the vertical lines | are the input variables, and after the vertical lines are the important learnable weights. In subsequent formulas, each vertical line means the same.

After processing each decoupled relational subgraph, UGAD learns the importance (weights) of different relations collaboratively, instead of dealing with each relational subgraph independently. It fuses the effects of these relations on anomaly detection through a set of learnable weight parameters  $a^r$  learnable weights as follows:

$$\tilde{\mathcal{X}}_{ma}^k = \sum_{r=1}^R a^r \mathcal{X}_{ma}^{r,k}, \quad (3)$$

where  $a^r$  is initially randomized using a normal distribution, and continuously optimized through the model's self-supervised training.

Finally, to optimize the attribute reconstruction, we compute the reconstruction error between the aggregated node attributes and the original attributes of the masked nodes as follows:

$$\mathcal{L}_A = \sum_{k=1}^K \frac{1}{|\mathcal{V}_{ma}^k|} \sum_{v_i \in \mathcal{V}_{ma}^k} \left( 1 - \frac{\tilde{\mathcal{X}}_{ma}^k(i)^\top x(i)}{\|\tilde{\mathcal{X}}_{ma}^k(i)\| \cdot \|x(i)\|} \right)^\eta, \quad \eta \geq 1, \quad (4)$$

which is the average reconstruction loss of all masked nodes.  $\mathcal{V}_{ma}^k$  is the  $k$ -th masked node subset,  $\tilde{\mathcal{X}}_{ma}^k(i)$  denotes the  $i$ -th reconstructed node attribute vector in  $\mathcal{X}_{ma}^{r,k}$ ,  $x(i)$  denotes the  $i$ -th original node attribute vector in  $\mathcal{X}$ . The scaling factor  $\eta$  is a hyperparameter that can be adjusted on different datasets.

2) *Structure Reconstruction*: Besides attribute anomalies, structural anomalies are also more difficult to recognize, they can be camouflaged by mimicking the attributes of normal nodes. However, structural inconsistencies are reflected in the

connections, and if the target node is not well reconstructed structurally, then it is likely to be anomalous.

Similar to node attribute reconstruction, we capitalize on the inconsistency of the structure space and introduce a structural (edge) masking mechanism that works to break short-range connections, causing nodes to look elsewhere for evidence that suits them. We set masking ratios as  $r_m$  to randomly sample an edge subset  $\mathcal{E}_{ms}^r$  from the edges observed in the subgraph and then obtain the corresponding perturbed subgraph as follows:

$$\mathcal{G}_{ms}^r = (\mathcal{V}, \mathcal{E}^r \setminus \mathcal{E}_{ms}^r, \mathcal{X}), \quad (5)$$

where  $\mathcal{E}^r \setminus \mathcal{E}_{ms}^r$  denotes the remaining edges set after edge masking in the  $r$ -th subgraph. Similarly, We utilize the same random sampling method as attribute masking to select the masked edges. We repeat the structure masking strategy on all relational subgraphs for  $K$  times to finally generate a set of masked subgraphs  $\mathcal{G}_{ms}^r = \{\mathcal{G}_{ms}^{r,1}, \mathcal{G}_{ms}^{r,2}, \dots, \mathcal{G}_{ms}^{r,K}\}$  for each relational subgraph  $\mathcal{G}^r$ , which are further fed into the GNN-based encoder and decoder to learn the node attribute:

$$\mathcal{X}_{ms}^{r,k} = Dec(Enc(\mathcal{V}, \mathcal{E}^r \setminus \mathcal{E}_{ms}^r | \mathbf{W}_{enc2}^{r,k}), \mathcal{E}^r \setminus \mathcal{E}_{ms}^r | \mathbf{W}_{dec2}^{r,k}), \quad (6)$$

where  $\mathcal{X}_{ms}^{r,k} \in \mathbb{R}^{|\mathcal{V}| \times f}$  is the output of the attribute decoder in the  $k$ -th masking repeat of the  $r$ -th relational subgraph,  $\mathbf{W}_{enc2}^{r,k} \in \mathbb{R}^{f \times d_h}$  and  $\mathbf{W}_{dec2}^{r,k} \in \mathbb{R}^{d_h \times f}$  are the trainable weight matrices. In contrast to the reconstruction goal of attribute masking, we use the edge set of the  $k$ -th masked sampling subgraph of the  $r$ -th relational subgraph,  $\mathcal{E}_{ms}^{r,k}$ , as a self-supervised signal to recover the original subgraph structure by predicting the masked edges with the cross-entropy function as follows:

$$\mathcal{L}_S^r = \sum_{k=1}^K \sum_{(v,u) \in \mathcal{E}_{ms}^{r,k}} \log \frac{\exp(g(v, u))}{\sum_{(v,u') \in \mathcal{E}_{ms}^{r,k}} \exp(g(v, u'))}, \quad (7)$$

where  $g(v, u) = \mathcal{X}_{ms}^{r,k}(v)^\top \mathcal{X}_{ms}^{r,k}(u)$  calculates the estimated probability of link between node  $v$  and  $u$ , and then we can obtain the reconstructed adjacent matrix  $\tilde{\mathbf{A}}_O^r$ . We introduce negative sampling to train a more generalized model by accumulating all edge prediction probabilities of the unmasked subgraphs in the denominator, making the model robust to external noise. Notably, the standard normalization in Eq. 4 is used to calculate the similarity between the reconstructed attribute features and the original attribute features. The softmax normalization in Eq. 7 is used to evaluate the probability of a link being reconstructed between two nodes.

Similar to Eq. 3, collaboratively considering the importance of different relational subgraphs for structure reconstruction, we aggregate all subgraph structure reconstruction losses together using a set of learnable weight parameters  $b^r$  as follows:

$$\mathcal{L}_S = \sum_{r=1}^R b^r \mathcal{L}_S^r, \quad (8)$$

where  $b^r$  is initially randomized and continuously optimized through the model's self-supervised training, similar to  $a^r$ .

The learned embedding captures anomalies in the attribute and structure space by jointly masking the attributes and edge

reconstruction of the subgraph. Finally, the training objective for the original-view graph reconstruction is as follows:

$$\mathcal{L}_O = \alpha \mathcal{L}_A + (1 - \alpha) \mathcal{L}_S, \quad (9)$$

where  $\alpha \in (0, 1)$  is the hyperparameter to balance the importance between attribute reconstruction loss  $\mathcal{L}_A$  and structure reconstruction loss  $\mathcal{L}_S$ .

### B. Augmented-view Graph Reconstruction

Due to the small number of anomalies, graphs containing anomalous nodes are usually unbalanced, which may disturb the detection of anomalous nodes. Therefore, we introduce two simplified graph masking strategies to generate two levels of augmented graphs, namely: attribute-level augmented graph and subgraph-level augmented graph, to reduce the redundant information in the original graph. Note that in the augmented-view graph reconstruction module, we do not actually adopt traditional graph data augmentation methods. Instead, we perform attribute-level augmentation by swapping the attributes of different nodes and subgraph-level augmentation through subgraph masking, without introducing new content.

1) *Attribute-level Augmented Graph Reconstruction*: For this module, we randomly select a subset of nodes  $\mathcal{V}_{na} \subset \mathcal{V}$  for replacement-based augmentation. The selected node features are adjusted as follows:

$$\tilde{x}(i) = \begin{cases} x(j), & i \in \mathcal{V}_{aa} \\ x(i), & i \in \mathcal{V} \setminus \mathcal{V}_{aa} \end{cases}. \quad (10)$$

We randomly select another node  $j$  and replace the original feature  $x(i)$  of  $i$  with the feature  $x(j)$  of node  $j$  if  $i \in \mathcal{V}_{aa}$ . Based on this strategy, we obtain the attribute-level augmented graph,  $\mathcal{G}_{aa}$ . Then we introduce the masking mechanism that only masks the augmented node set  $\mathcal{V}_{aa}$ , where the feature of each node  $i \in \mathcal{V}_{aa}$  is masked.

We repeat the above augmentation operation for  $K$  times to generate a collection of the attribute-level augmented graphs for each relational subgraph  $\mathcal{G}^r$ , denoted as  $\mathcal{G}_{aa}^r = \{\mathcal{G}_{aa}^{r,1}, \mathcal{G}_{aa}^{r,2}, \dots, \mathcal{G}_{aa}^{r,K}\}$ , where each  $\mathcal{G}_{aa}^{r,k} = (\mathcal{V}, \mathcal{E}^r, \tilde{\mathcal{X}}_{aa}^{r,k})$ , and  $\tilde{\mathcal{X}}_{aa}^{r,k}$  is the augmented attribute matrix generated each time. We feed each  $\mathcal{G}_{aa}^{r,k}$  into the attribute-level GMAE consisting of the simplified GCN encoder and decoder with a masking mechanism. Then we can obtain the reconstructed node embedding matrix  $\mathcal{X}_{na}^{r,k}$  as follows:

$$\mathcal{X}_{na}^{r,k} = Dec(Enc(\mathcal{V}, \mathcal{E}^r | \mathbf{W}_{enc3}^{r,k}), \mathcal{E}^r | \mathbf{W}_{enc3}^{r,k}). \quad (11)$$

Similarly, we aggregate all subgraph attributes by using the set of learnable weights  $a^r$  as follows:

$$\tilde{\mathcal{X}}_{aa}^k = \sum_{r=1}^R a^r \mathcal{X}_{aa}^{r,k}. \quad (12)$$

Therefore, the training objective for the attribute-level augmented-view graph reconstruction is defined as follows:

$$\mathcal{L}_{A\_Aug} = \frac{1}{|\mathcal{V}_{aa}^k|} \sum_{k=1}^K \sum_{v_i \in \mathcal{V}_{aa}^k} \left( 1 - \frac{\tilde{x}_{aa}^k(i)^\top x(i)}{\|\tilde{x}_{aa}^k(i)\| \cdot \|x(i)\|} \right)^\eta, \eta \geq 1, \quad (13)$$

where  $|\mathcal{V}_{aa}^k|$  is the  $k$ -th masked subset,  $\tilde{x}_{aa}^k(i)$  denotes the reconstructed node attribute vector in  $\tilde{\mathcal{X}}_{aa}^k$ ,  $x(i)$  denotes the original node attribute vector in  $\mathcal{X}$ .

2) *Subgraph-level Augmented Graph Reconstruction*: First, we propose a subgraph masking mechanism that employs a subgraph sampling strategy based on random walk with restart for subgraph sampling and masks these sampled subgraphs for each relational subgraph  $\mathcal{G}^r$  in  $\mathcal{G}$ . Then we obtain the subgraph-level augmented graphs collection  $\mathcal{G}_s^r = \{\mathcal{G}_s^{r,1}, \mathcal{G}_s^{r,2}, \dots, \mathcal{G}_s^{r,K}\}$ , where  $\mathcal{G}_s^{r,k} = (\mathcal{V}, \mathcal{E}^r \setminus \mathcal{E}_s^r, \mathcal{X}_s^{r,k})$ ,  $\mathcal{E}_s^r$  and  $\mathcal{X}_s^{r,k}$  are the edge subset and generated attribute matrix.

Subgraph-level augmentation can be considered as a specific combination of node attribute level and structure level augmentation. The reconstructed node attribute matrix  $\tilde{\mathcal{X}}_{sa}^k$  and structural adjacent matrix  $\tilde{\mathbf{A}}_{ss}^r$  are shown below, respectively:

$$\tilde{\mathcal{X}}_{sa}^k = \sum_{r=1}^R a^r \mathcal{X}_{sa}^{r,k}, \quad \tilde{\mathbf{A}}_{ss}^r = \sum_{k=1}^K \sigma((\tilde{\mathcal{X}}_{sa}^k)^\top \tilde{\mathcal{X}}_{sa}^k). \quad (14)$$

Then the subgraph-level augmented attribute and structure reconstruction loss values  $\mathcal{L}_{sa}$  and  $\mathcal{L}_{ss}$  is defined as follows:

$$\mathcal{L}_{sa} = \frac{1}{|\mathcal{V}_{sa}^k|} \sum_{k=1}^K \sum_{v_i \in \mathcal{V}_{sa}^k} \left( 1 - \frac{\tilde{x}_{sa}^k(i)^\top x(i)}{\|\tilde{x}_{sa}^k(i)\| \cdot \|x(i)\|} \right)^\eta, \eta \geq 1, \\ \mathcal{L}_{ss} = \sum_{r=1}^R b^r \sum_{k=1}^K \sum_{(v,u) \in \mathcal{E}_{ss}^{r,k}} \log \frac{\exp(g(v,u))}{\sum_{(v,u') \in \mathcal{E}_{ss}^{r,k}} \exp(g(v,u'))}, \quad (15)$$

where  $|\mathcal{V}_{sa}^k|$  is the  $k$ -th masked subset,  $\tilde{x}_{sa}^k(i)$  and  $x(i)$  are the attribute-level augmented embedding and original node attribute respectively, and  $g(v,u) = x_s^{r,k}(v)^\top x_s^{r,k}(u)$  denotes the estimated probability of the link between node  $v$  and  $u$ .

Finally, the training objective for the subgraph-level augmented-view graph reconstruction is defined as follows:

$$\mathcal{L}_{S\_Aug} = \beta \mathcal{L}_{sa} + (1 - \beta) \mathcal{L}_{ss}. \quad (16)$$

where  $\beta \in (0, 1)$  is the hyperparameter to balance the importance between attribute and structure reconstruction loss,  $\mathcal{L}_{sa}$  and  $\mathcal{L}_{ss}$ , in the subgraph-level augmentation.

It is worthwhile to emphasize that normal nodes tend to have more similar features than their neighbors, while anomalous nodes exhibit greater feature differences. Through masking and GNN-based reconstruction, normal nodes are more likely to be accurately reconstructed, whereas anomalous nodes are less likely to be. Therefore, we improve the model's ability to identify anomalies by employing different masking mechanisms with graph autoencoder.

### C. Dual-view Contrastive Learning

Dual-view contrastive learning is defined between the original view and the augmented view, to learn more representative and intrinsic node embeddings, which helps capture further anomaly information. Specifically, we optimize the node attribute under joint loss by comparing the original-view graph with the attribute-level augmented-view graph and the

subgraph-level augmented-view graph, respectively. The node attribute of node  $i$  in the original view forms a positive pair with the augmented view and a negative pair with the attribute of node  $j$  in the original and augmented views. We use the following loss function to optimize contrastive learning:

$$\begin{aligned}\mathcal{L}_{cl}^{oa} &= -\sum_{i=1}^{|V|} \log \frac{e^{\tilde{x}_{ma}(i) \cdot \tilde{x}_{aa}(i)}}{e^{\tilde{x}_{ma}(i) \cdot \tilde{x}_{ma}(j)} + e^{\tilde{x}_{ma}(i) \cdot \tilde{x}_{aa}(j)}}, \\ \mathcal{L}_{cl}^{os} &= -\sum_{i=1}^{|V|} \log \frac{e^{\tilde{x}_{ma}(i) \cdot \tilde{x}_{sa}(i)}}{e^{\tilde{x}_{ma}(i) \cdot \tilde{x}_{ma}(j)} + e^{\tilde{x}_{ma}(i) \cdot \tilde{x}_{sa}(j)}},\end{aligned}\quad (17)$$

where  $\mathcal{L}_{cl}^{oa}$  represents the contrastive loss between the original-view graph and the attribute-level augmented-view graph,  $\mathcal{L}_{cl}^{os}$  represents the contrastive loss between the original-view graph and the subgraph-level augmented-view graph. The final loss dual-view contrastive learning is  $\mathcal{L}_{CL} = \mathcal{L}_{cl}^{oa} + \mathcal{L}_{cl}^{os}$ .

#### D. Optimization Objective

Putting it all together, we have the overall loss function in the training stage is as follows:

$$\mathcal{L} = \mathcal{L}_O + \lambda \mathcal{L}_{A\_Aug} + \mu \mathcal{L}_{S\_Aug} + \Theta \mathcal{L}_{CL}, \quad (18)$$

where  $\lambda$ ,  $\mu$ , and  $\Theta$  are hyperparameters that measure the importance of diverse augmented views and contrastive learning.

Based on the final training loss  $\mathcal{L}$ , we train several autoencoder modules, sort the nodes based on their anomaly scores,  $S(i)$ , and treat the nodes with higher  $S(i)$  as anomalous nodes. For both original-view and augmented-view graphs, we use the following formula to calculate and finally take the arithmetic average of multiple views as the anomaly score of node  $v_i$ :

$$S(i)_* = \varepsilon \cdot \|\tilde{x}_*(i) - x(i)\|_1 + (1-\varepsilon) \cdot \frac{1}{R} \sum_{r=1}^R \left\| \tilde{\zeta}_*^r(i) - \zeta^r(i) \right\|_2, \quad (19)$$

where  $*$  denotes the specific original ( $O$ ), attribute-level augmented ( $A\_Aug$ ), or subgraph-level augmented ( $S\_Aug$ ) graph,  $\|\cdot\|_1$  denotes the Euclidean norm of a vector,  $\|\cdot\|_2$  denotes the L1-norm of the vector,  $\tilde{\zeta}_*^r(i)$  and  $\zeta^r(i)$  represent the  $i$ -th row of the specific reconstructed structure matrix  $\tilde{\mathbf{A}}_*^r$  and original structure matrix  $\mathbf{A}^r$ , respectively. Similarly,  $\tilde{x}_*(i)$  and  $x(i)$  are reconstructed attribute vector and original attribute vector of the node  $i$ , respectively. Therefore, the anomaly score  $S(i)$  of node  $i$  is the mean value of all  $S(i)_*$ .

#### E. Unsupervised Anomaly Score Threshold Selection Strategy

For the unsupervised graph anomaly detection task, since the nodes' label (normal or abnormal) is unknown, a common approach is to compute the anomaly score for each node and rank them in order of the anomaly score from high to low. Nodes with high anomaly scores are considered anomalous nodes. However, determining a more accurate anomaly score threshold has always been a difficult problem in UGAD.

To determine an anomaly score threshold for unsupervised graph anomaly detection, we propose a strategy that combines moving average smoothing and inflection point detection. This approach works directly on the ordered anomaly score

sequence, without relying on ground truth information from the test set (e.g., the number of anomalous nodes), making it suitable for real unsupervised scenarios.

Given the learned anomaly score set for  $|\mathcal{V}|$  nodes, we first sort the scores in descending order to form  $S = \{s(1), s(2), \dots, s(|\mathcal{V}|)\}$ , where  $s(1) \geq s(2) \geq \dots \geq s(|\mathcal{V}|)$ . The sorted sequence reflects the relative magnitude of anomaly scores, with higher scores more likely corresponding to anomalous nodes. To mitigate the effects of noise and ensure a smooth transition in the sequence, we apply a moving average smoothing technique. For a given sliding window size  $w$ , the smoothed score sequence  $\bar{S}$  is computed as:

$$\bar{s}(i) = \frac{1}{w} \sum_{j=i}^{i+w-1} s(j), \quad i = 1, 2, \dots, |\mathcal{V}| - w + 1. \quad (20)$$

The choice of  $w$  balances noise reduction and the preservation of meaningful variations in the scores. A practical guideline is to set  $w = \max(\lfloor 0.0001|\mathcal{V}|\rfloor, 5)$ , which works well across different data scales. After smoothing, we calculate the first-order and second-order differences of the sequence to analyze its structural changes. The first-order difference is:

$$\Delta_1(i) = \bar{s}(i) - \bar{s}(i+1), \quad i = 1, 2, \dots, |\mathcal{V}| - w, \quad (21)$$

while the second-order difference is defined as follows:

$$\Delta_2(i) = \Delta_1(i) - \Delta_1(i+1), \quad i = 1, 2, \dots, |\mathcal{V}| - w - 1. \quad (22)$$

Here,  $\Delta_1(i)$  captures the local decrease in scores, and  $\Delta_2(i)$  identifies changes in the rate of decrease. The second-order difference captures the inflection point where the decline in anomaly scores transitions from steep (anomalous nodes) to stable (normal nodes). The inflection point  $\mathcal{T}$  is identified as the index  $i$  where the magnitude of  $\Delta_2(i)$  reaches its maximum:

$$\mathcal{T} = \arg \max_i |\Delta_2(i)|, \quad i = 1, 2, \dots, |\mathcal{V}| - w - 1, \quad (23)$$

which corresponds to the region where the anomaly score sequence transitions from a steep decline to a plateau. The anomaly score threshold  $s(\mathcal{T})$  is then defined as the smoothed score at the inflection point  $\mathcal{T}$ . If there exists several selectable points consistent with Eq. 23, we select the one with the smallest difference from  $\bar{s}(|\mathcal{V}|)$  as  $\mathcal{T}$ . Therefore, nodes with scores  $s(i) \geq s(\mathcal{T})$  are considered anomalous, while those with scores  $s(i) < s(\mathcal{T})$  are deemed normal.

We believe that a good anomaly detection model should be able to clearly distinguish between anomalous and normal nodes based on anomaly scores. In other words, the anomaly scores, when sorted in descending order, should gradually stabilize and show a clear inflection point. Before the inflection point (with relatively higher anomaly scores), the nodes are likely to be anomalous, while after the inflection point (with smaller and less differentiated scores), the nodes should be considered normal. This method leverages the distribution of anomaly scores to identify a natural threshold, without requiring any ground truth labels. The combination of smoothing and inflection point detection ensures the approach is robust to noise while effectively distinguishing between anomalous and normal nodes.

### F. Time complexity Analysis

The proposed UMGAD consists of three critical components: original-view graph reconstruction, augmented-view graph reconstruction, and dual-view contrastive learning. In original-view graph reconstruction, the time complexity of GMAE is  $O(|\mathcal{V}| \times L \times f)$ , and the time complexity of attention aggregation operation is  $O(|\mathcal{V}| \times d_h \times f \times R)$ , where  $|\mathcal{V}|$  denotes the number of nodes, and  $L$  represents the number of Simplified GCN layers,  $d_h$  and  $f$  denote the dimension of latent vectors and the size of node attribute,  $R$  is the number of relational subgraphs. The overall time complexity of original-view graph reconstruction is  $O(|\mathcal{V}| \times f \times (L + d_h \times R))$ . For augmented-view graph reconstruction, the overall time complexity is  $O(|\mathcal{V}| \times f \times (L + d_h \times R))$ . The time complexity for dual-view contrastive learning is  $O(|\mathcal{V}| \times f^2 + |\mathcal{V}| \times f)$ . Hence, the entire time complexity of the proposed UMGAD is approximately  $O(|\mathcal{V}| \times f \times (L + d_h \times R + f))$ .

## V. EXPERIMENTS

In this section, we evaluate the performance of our proposed method through extensive experiments and answer the following questions:

- **(RQ1)** How does UMGAD effectively alleviate the difficulty of selecting anomaly score thresholds in UGAD?
- **(RQ2)** How does UMGAD perform compared to other GAD methods in real unsupervised scenarios?
- **(RQ3)** What are the effects of different modules in UMGAD on performance?
- **(RQ4)** How do different hyperparameter settings affect the performance?
- **(RQ5)** How does UMGAD perform compared to other GAD methods in the scenario of threshold selection with ground truth leakage?
- **(RQ6)** How does UMGAD perform in terms of time efficiency compared to SOTA methods?

### A. Experimental Settings

1) *Dataset*: We have conducted experiments on two datasets injected with synthetic anomalies: Retail\_Rocket [47] (Retail for short) and Alibaba [48], and two real-world publicly available datasets with anomalies: Amazon [5] and YelpChi [49]. The detailed description of these datasets is shown as follows. Three datasets are adopted for evaluation:

- **Retail\_Rocket (Retail for short)**. This is a benchmark dataset collected from the RetailRocket recommendation system. In this dataset, interactive relations between users and items include page views (View), add-to-cart (Cart), and transactions (Buy).
- **Alibaba**. This dataset is collected from Alibaba, one of the largest e-commerce platforms in China. It contains three interactive relations between users and items, *i.e.*, page view (View), add to cart (Cart), and purchase (Buy).
- **Amazon**. This dataset is collected from Amazon, it contains three interactive relations among users: U-P-U links users reviewing at least one product, U-S-U links users having at

TABLE I: Statistical information of evaluation datasets. #Ano. denotes the number of anomalies, (I) represents the injected anomalies, and (R) represents the real anomalies.

Datasets	#Nodes	#Ano. (I/R)	Relation Type	#Edges
Retail	32,287	300 (I)	View	75,374
			Cart	12,456
			Buy	9,551
Alibaba	22,649	300 (I)	View	34,933
			Cart	6,230
			Buy	4,571
Amazon	11,944	821 (R)	U-P-U	175,608
			U-S-U	3,566,479
			U-V-U	1,036,737
YelpChi	45,954	6674 (R)	R-U-R	49,315
			R-S-R	3,402,743
			R-T-R	573,616

least one identical star rating within a week, U-V-U links linguistically similar users.

- **YelpChi**. This dataset is collected from Yelp, it contains three interactive relations among users: R-U-R connects the reviews posted by the same user, R-S-R connects reviews that have the same identical star rating, R-T-R connects reviews that posted in the same term.

Specifically, for synthetic anomalies, we follow the approach from [8] to introduce both structural and attribute anomalies. When injecting structural anomalies, we specify that a clique of size  $m$  is introduced, *i.e.*, if  $m$  nodes are randomly selected from the network and then these nodes are made fully connected, all  $m$  nodes in the clique are considered as anomalies. We iteratively repeat this process until  $n$  factions are generated and the total number of structural anomalies is  $m \times n$ . Correspondingly, when injecting attribute anomalies, we first randomly select additional  $m \times n$  nodes as attribute perturbation candidates. For each selected node  $i$ , we randomly select another  $k$  nodes from the data and select the node  $j$  whose attribute among the  $k$  nodes deviates most from node  $i$  by maximizing the Euclidean distance  $\|x_i - x_j\|^2$ . Then, we change the attribute  $x_i$  of node  $i$  to  $x_j$ . Additionally, for datasets containing real anomalies, we directly use the publicly available datasets from [9].

- 2) *Baselines*: We mainly compare five categories of methods on the unsupervised GAD task including the traditional method Radar [27].

### Traditional GAD Method:

- **Radar** [27]: It is a learning framework for characterizing the residuals of attribute information in anomaly detection and its consistency with network information.

### Specific GAD Methods:

- **ComGA** [28]: It is a community-aware anomaly detection framework that enhances GNNs through community-based segmentation and feature learning.
- **RAND** [36]: It integrates reinforced neighborhood selection and improves the message-passing mechanism for unsupervised graph anomaly detection.

- **TAM** [29]: It learns node embeddings for anomaly detection by maximizing local affinity and removing non-homogeneous edges to reduce bias.

#### CL-based GAD Methods:

- **CoLA** [41]: It proposes a GNN-based contrastive model that captures high-dimensional attributes and local structures using a novel sampling method.
- **ANEMONE** [50]: It employs a GNN encoder with multi-scale contrastive learning to capture graph patterns and a statistical estimator to detect node anomalies based on consistency.
- **Sub-CR** [42]: It is a self-supervised framework combining multi-view comparison and attribute reconstruction to detect anomalies on attribute networks.
- **ARISE** [51]: It is a graph anomaly detection model that identifies anomalies by learning substructures in attribute networks.
- **SL-GAD** [52]: It uses contextual views with generative attribute regression and multi-view comparative learning to detect attribute, structural, and mixed anomalies.
- **PREM** [53]: It includes a preprocessing module and an isochronous bit matching module to eliminate message-passing during training, using a simple contrastive loss to reduce training time and memory usage.
- **GCCAD** [30]: It proposes a pre-training strategy to address label scarcity by generating pseudo anomalies through graph corruption.
- **GRADATE** [31]: It is a multi-view, multi-scale contrastive learning framework that captures features to detect complex structural anomalies.
- **VGOD** [32]: It is a variance-based graph outlier detection method that combines variance modeling and attribute reconstruction for balanced detection.

#### GAE-based GAD Methods:

- **GCNAE** [54]: It is an unsupervised model using a variational graph autoencoder (VGAE) with GCN encoding and latent variables to learn graph embeddings.
- **DOMINANT** [44]: It learns node embeddings using GCN to model graph topology and attributes, then reconstructs the original data with a deep autoencoder.
- **AnomalyDAE** [55]: It is a joint representation learning model for anomaly detection using dual self-encoders to capture interactions between structure and node attributes.
- **AdONE** [56]: It is an unsupervised AE approach with adversarial learning to separately learn network structure and attribute embeddings, minimizing the impact of outliers.
- **GAD-NR** [45]: It combines neighborhood reconstruction for GAD problem, aiming to reconstruct a node's entire neighborhood, including its local structure and attributes.
- **ADA-GAD** [33]: It is a two-stage anomaly denoising autoencoder framework that reduces anomalies, trains a graph autoencoder, and applies node anomaly distribution regularization to prevent overfitting.
- **GADAM** [57]: It is a local inconsistency mining approach that resolves conflicts with GNN messaging and enhances

anomaly detection through improved message passing.

#### MV Methods:

- **AnomMAN** [46]: It is a GCN-based framework for anomaly detection on multi-view attribute networks, using attention to fuse information across views.
- **DualGAD** [13]: It is a self-supervised model combining generative and contrastive modules with masked subgraph reconstruction for improved node-level anomaly detection.

3) *Implementation Details*: We implement all baselines according to their provided code or utilizing the PyGOD toolkit. We set the epoch number, dropout rate, and weight decay to 20, 0.1, and 0.01, respectively, and the embedding dimension  $d$  to 32, and our method uses Simplified GCN as the encoder and decoder. For Amazon and YelpChi with real anomalies, the number of encoder layers is set to 2 and the depth of the decoder is set to 1. For Retail and Alibaba with synthetic anomalies, the number of encoder and decoder layers are both set to 1. The pre-training epoch and the retention epoch are both set to 20. AUC (area under the ROC curve) and Macro-F1 are used as performance metrics. All experiments are performed on 4 RTX 4090 GPUs with 24GB memory.

#### B. Anomaly Score Threshold Selection for Unsupervised Anomaly Detection (RQ1)

The results on four datasets are shown in Fig. 2, which shows the trend of the ranked node anomaly scores for the best-performing baselines, TAM, ADA-GAD, GADAM, AnomMAN, and for our UMGAD, respectively. We can see that compared with the other four best-performing baselines, the curve of our UMGAD can converge quickly (become stable) to a position closer to the actual number of anomalies in the datasets. It allows UMGAD to distinguish better the anomaly scores of anomalous nodes from those of normal nodes, and thus be able to identify anomalies more accurately. Notably, a robust anomaly detection model should effectively separate anomalous nodes from normal ones by leveraging anomaly scores. Specifically, the anomaly scores, when arranged in descending order, ought to display a distinct inflection point where they stabilize. Nodes with higher anomaly scores preceding this inflection point are likely to be anomalous, whereas those with lower, more uniform scores beyond this point can be viewed as normal. Therefore, we use the anomaly score at inflection point of the fitting curve as the anomaly threshold. The number of anomalous nodes corresponding to the selected threshold is very close to the real number of anomalies which can be identified by ground truth information, which proves that our method can effectively alleviate the difficult problem of selecting anomaly thresholds.

Our proposed anomaly threshold selection strategy is the first truly unsupervised method. It does not require any ground-truth information from the test set, making it a fair and objective model evaluation approach. Therefore, the experimental results in Table II are objective. Although the results in Table IV are generally better than those in Table II, they are not objective, as ground-truth information from the test set

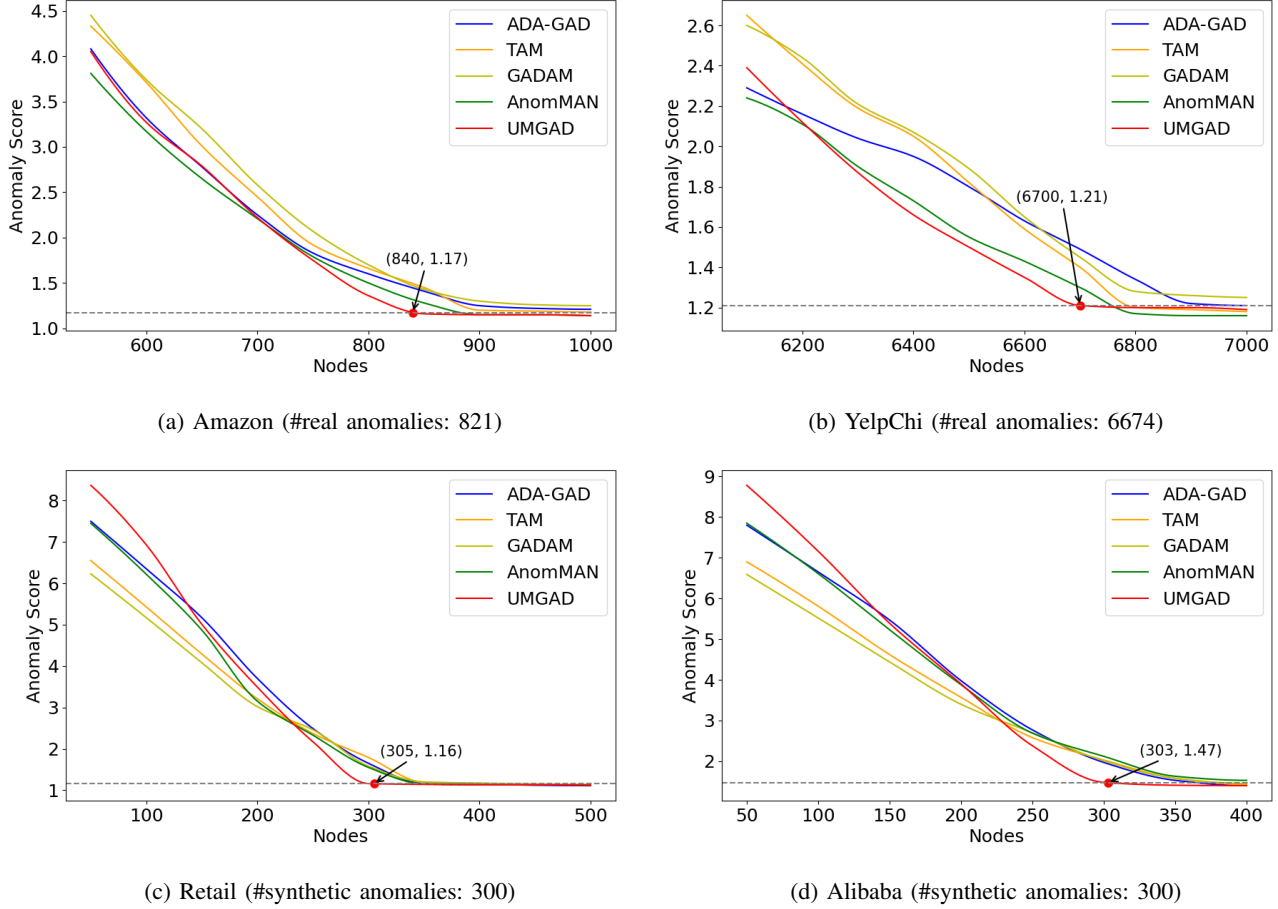


Fig. 2: Visualization of ranked node anomaly scores for SOTA methods on four datasets.

(e.g., the number of anomalous nodes) is used when selecting anomaly thresholds.

### C. Performance Comparison in the Real Unsupervised Scenario (RQ2)

Next, we evaluate the performance of our UMGAD and all baselines in real unsupervised scenarios. The experimental results are shown in Table II. The best results are highlighted in bold, and the second-best results are underlined.

As we can see, our UMGAD obtains the optimal performance, significantly achieves 13.48%, and 11.68% average improvement in terms of AUC and macro-F1 across four datasets. We can draw the following conclusions: First, according to our proposed threshold selection strategy and the node anomaly score curves in Fig. 2, the number of detected anomalies corresponding to our selected thresholds is the closest to the real situation compared to other methods. Second, our UMGAD method considers the multi-relational correlation between nodes, and collaboratively combines GAEs with various masking mechanisms across different types of relations, effectively capturing diverse anomaly signals in both original and augmented views. Therefore, the anomaly scores of anomalous nodes can be better distinguished from those of normal nodes.

### D. Ablation Study (RQ3)

To evaluate the effectiveness of each component in UMGAD, we further conduct ablation studies on different variants. Specifically, we generate five variants as follows:

- **w/o M** removes the GMAE module and uses corresponding the GAE module instead.
- **w/o O** removes the original-view graph-masked autoencoder and only detects augmented graphs.
- **w/o A** removes the augmented-view graph-masked autoencoder and only detect original graphs.
- **w/o NA** excludes the node attribute-level augmentation.
- **w/o SA** excludes the subgraph-level augmentation.
- **w/o DCL** excludes the dual-view contrastive learning.

Table III presents the results of model variants on four datasets in real unsupervised scenarios. All five variants underperform UMGAD in terms of AUC and macro-F1, under-scoring the necessity and effectiveness of the proposed components. Among them, **w/o M** performs the worst, highlighting the importance of the graph-masked autoencoder (GMAE) in GAD tasks. Ordinary GAE struggles to accurately reconstruct the attributes and structural features of anomalous nodes, leading to suboptimal anomaly detection performance. **w/o O** outperforms **w/o M** and **w/o A**, emphasizing the critical role of

TABLE II: Performance comparison of all models on four datasets in the real unsupervised scenario.

Method		Retail		Alibaba		Amazon		YelpChi	
		AUC	Macro-F1	AUC	Macro-F1	AUC	Macro-F1	AUC	Macro-F1
Trad.	Radar [IJCAI'17]	0.625 $\pm$ 0.002	0.533 $\pm$ 0.007	0.659 $\pm$ 0.003	0.560 $\pm$ 0.008	0.582 $\pm$ 0.007	0.525 $\pm$ 0.004	0.502 $\pm$ 0.003	0.485 $\pm$ 0.011
MPI	ComGA [WSDM'22]	0.626 $\pm$ 0.015	0.553 $\pm$ 0.018	0.591 $\pm$ 0.003	0.573 $\pm$ 0.006	0.661 $\pm$ 0.006	0.691 $\pm$ 0.013	0.514 $\pm$ 0.001	0.491 $\pm$ 0.001
	RAND [ICDM'23]	0.665 $\pm$ 0.007	0.622 $\pm$ 0.010	0.692 $\pm$ 0.002	0.603 $\pm$ 0.007	0.660 $\pm$ 0.004	0.687 $\pm$ 0.008	0.525 $\pm$ 0.005	0.501 $\pm$ 0.002
	TAM [NeurIPS'24]	0.688 $\pm$ 0.006	0.650 $\pm$ 0.007	0.712 $\pm$ 0.004	0.660 $\pm$ 0.008	0.763 $\pm$ 0.011	0.637 $\pm$ 0.008	0.546 $\pm$ 0.007	0.538 $\pm$ 0.008
CL	CoLA [TNNLS'21]	0.554 $\pm$ 0.013	0.513 $\pm$ 0.011	0.570 $\pm$ 0.011	0.541 $\pm$ 0.018	0.582 $\pm$ 0.008	0.522 $\pm$ 0.005	0.444 $\pm$ 0.003	0.468 $\pm$ 0.007
	ANEMONE [CIKM'21]	0.630 $\pm$ 0.004	0.589 $\pm$ 0.009	0.651 $\pm$ 0.002	0.581 $\pm$ 0.008	0.622 $\pm$ 0.013	0.550 $\pm$ 0.014	0.503 $\pm$ 0.011	0.492 $\pm$ 0.018
	Sub-CR [IJCAI'22]	0.650 $\pm$ 0.006	0.594 $\pm$ 0.008	0.652 $\pm$ 0.017	0.599 $\pm$ 0.012	0.599 $\pm$ 0.005	0.530 $\pm$ 0.007	0.489 $\pm$ 0.012	0.490 $\pm$ 0.013
	ARISE [TNNLS'23]	0.671 $\pm$ 0.011	0.635 $\pm$ 0.017	0.708 $\pm$ 0.019	0.619 $\pm$ 0.011	0.692 $\pm$ 0.009	0.612 $\pm$ 0.006	0.532 $\pm$ 0.002	0.503 $\pm$ 0.004
	SL-GAD [TKDE'21]	0.658 $\pm$ 0.018	0.596 $\pm$ 0.016	0.700 $\pm$ 0.008	0.611 $\pm$ 0.009	0.653 $\pm$ 0.008	0.585 $\pm$ 0.003	0.522 $\pm$ 0.005	0.484 $\pm$ 0.007
	PREM [ICDM'23]	0.661 $\pm$ 0.008	0.609 $\pm$ 0.009	0.680 $\pm$ 0.016	0.607 $\pm$ 0.008	0.658 $\pm$ 0.018	0.588 $\pm$ 0.003	0.521 $\pm$ 0.008	0.493 $\pm$ 0.006
	GCCAD [TKDE'22]	0.665 $\pm$ 0.011	0.611 $\pm$ 0.006	0.701 $\pm$ 0.006	0.630 $\pm$ 0.004	0.662 $\pm$ 0.007	0.591 $\pm$ 0.012	0.522 $\pm$ 0.013	0.497 $\pm$ 0.007
	GRADATE [AAAI'23]	0.683 $\pm$ 0.004	0.644 $\pm$ 0.004	0.702 $\pm$ 0.007	0.642 $\pm$ 0.009	0.730 $\pm$ 0.002	0.661 $\pm$ 0.012	0.540 $\pm$ 0.001	0.521 $\pm$ 0.003
	VGOD [ICDE'23]	0.680 $\pm$ 0.002	0.639 $\pm$ 0.003	0.710 $\pm$ 0.013	0.644 $\pm$ 0.015	0.724 $\pm$ 0.001	0.702 $\pm$ 0.006	0.538 $\pm$ 0.009	0.510 $\pm$ 0.002
GAE	DOMINANT [arXiv'16]	0.621 $\pm$ 0.009	0.577 $\pm$ 0.011	0.609 $\pm$ 0.008	0.549 $\pm$ 0.012	0.621 $\pm$ 0.005	0.581 $\pm$ 0.007	0.500 $\pm$ 0.005	0.490 $\pm$ 0.005
	GCNAE [SDM'19]	0.623 $\pm$ 0.007	0.579 $\pm$ 0.010	0.624 $\pm$ 0.007	0.564 $\pm$ 0.011	0.607 $\pm$ 0.017	0.583 $\pm$ 0.010	0.502 $\pm$ 0.010	0.494 $\pm$ 0.008
	AnomalyDAE [ICASSP'20]	0.618 $\pm$ 0.003	0.525 $\pm$ 0.005	0.665 $\pm$ 0.007	0.571 $\pm$ 0.008	0.634 $\pm$ 0.015	0.588 $\pm$ 0.012	0.523 $\pm$ 0.016	0.496 $\pm$ 0.010
	AdONE [WSDM'20]	0.621 $\pm$ 0.012	0.565 $\pm$ 0.010	0.641 $\pm$ 0.004	0.579 $\pm$ 0.004	0.649 $\pm$ 0.008	0.601 $\pm$ 0.009	0.520 $\pm$ 0.005	0.505 $\pm$ 0.003
	GAD-NR [WSDM'24]	0.681 $\pm$ 0.006	0.632 $\pm$ 0.005	0.707 $\pm$ 0.007	0.658 $\pm$ 0.010	0.752 $\pm$ 0.006	0.681 $\pm$ 0.005	0.540 $\pm$ 0.002	0.531 $\pm$ 0.008
	ADA-GAD [AAAI'24]	0.688 $\pm$ 0.003	0.650 $\pm$ 0.002	0.715 $\pm$ 0.002	0.663 $\pm$ 0.002	0.754 $\pm$ 0.001	0.687 $\pm$ 0.003	0.545 $\pm$ 0.006	0.530 $\pm$ 0.007
	GADAM [ICLR'24]	0.690 $\pm$ 0.008	0.644 $\pm$ 0.008	0.712 $\pm$ 0.001	0.656 $\pm$ 0.002	0.756 $\pm$ 0.004	0.687 $\pm$ 0.008	0.545 $\pm$ 0.005	0.535 $\pm$ 0.009
MV	AnomMAN [IS'23]	0.688 $\pm$ 0.005	0.645 $\pm$ 0.008	0.710 $\pm$ 0.006	0.650 $\pm$ 0.009	0.758 $\pm$ 0.005	0.689 $\pm$ 0.007	0.542 $\pm$ 0.006	0.536 $\pm$ 0.004
	DualGAD [IS'24]	0.688 $\pm$ 0.007	0.647 $\pm$ 0.003	0.712 $\pm$ 0.005	0.653 $\pm$ 0.004	0.758 $\pm$ 0.002	0.688 $\pm$ 0.006	0.542 $\pm$ 0.003	0.538 $\pm$ 0.008
	<b>UMGAD</b>	<b>0.770<math>\pm</math>0.009</b>	<b>0.722<math>\pm</math>0.005</b>	<b>0.825<math>\pm</math>0.006</b>	<b>0.740<math>\pm</math>0.006</b>	<b>0.878<math>\pm</math>0.005</b>	<b>0.779<math>\pm</math>0.004</b>	<b>0.608<math>\pm</math>0.001</b>	<b>0.597<math>\pm</math>0.004</b>
	<i>Improvement</i>	11.92% $\uparrow$	11.08% $\uparrow$	15.38% $\uparrow$	11.61% $\uparrow$	15.07% $\uparrow$	13.06% $\uparrow$	11.56% $\uparrow$	10.97% $\uparrow$

TABLE III: The comparison of UMGAD and its variants on AUC and macro-F1 (F1 for short) metrics.

Dataset Metrics	Retail		Alibaba		Amazon		YelpChi	
	AUC	F1	AUC	F1	AUC	F1	AUC	F1
w/o <i>M</i>	0.712	0.669	0.783	0.689	0.829	0.716	0.571	0.556
w/o <i>O</i>	0.720	0.682	0.788	0.696	0.835	0.727	0.577	0.565
w/o <i>A</i>	0.714	0.670	0.782	0.691	0.827	0.719	0.571	0.558
w/o <i>NA</i>	0.731	0.690	0.795	0.706	0.842	0.735	0.582	0.575
w/o <i>SA</i>	0.726	0.685	0.788	0.701	0.839	0.730	0.580	0.567
w/o <i>DCL</i>	0.748	0.702	0.806	0.718	0.848	0.755	0.588	0.577
<b>UMGAD</b>	<b>0.770</b>	<b>0.722</b>	<b>0.825</b>	<b>0.740</b>	<b>0.878</b>	<b>0.779</b>	<b>0.608</b>	<b>0.597</b>

the original multiplex heterogeneous graph. Relying solely on the augmented graph risks losing crucial anomaly information. The results for *w/o NA* and *w/o SA* further demonstrate that the augmented-view GMAE is effective in capturing anomalous information. Changes to node attributes and structural features in the augmented graph help mitigate the homogeneity trap common in GNN-based autoencoders. Finally, while *w/o CDL* performs the best among all variants, it still falls short of UMGAD, confirming the significant contribution of dual-view contrastive learning in optimizing node representations.

#### E. Parameter Sensitivity Analysis (RQ4)

1) *The effect of hyperparameters  $\lambda$ ,  $\mu$  and  $\Theta$  in the final loss function:*  $\lambda$ ,  $\mu$  and  $\Theta$  correspond to the importance parameters of the two enhanced views and dual-view contrastive learning, respectively. Considering node attribute-level and subgraph-level enhanced views on top of the original view can improve

the model performance, and the results of the parameter sensitivity experiments are shown in Fig. 3. The model performance is optimal when  $\lambda$  and  $\mu$  are set to 0.3 and 0.3, 0.3 and 0.4, 0.4 and 0.4, and 0.4 and 0.5 on the four datasets, respectively. Besides, our UMGAD tends to perform well by setting  $\Theta$  to 0.1 across all datasets.

2) *The effect of masking ratio  $r_m$  and masking subgraph size  $|\mathcal{V}_m|$ :* To investigate how subgraph size  $|\mathcal{V}_m|$  (number of nodes) and masking ratio  $r_m$  affect model performance, we test  $|\mathcal{V}_m| \in \{4, 8, 12, 16\}$  and  $r_m \in \{20\%, 40\%, 60\%, 80\%\}$  on four datasets. As shown in Fig. 4, YelpChi and Amazon achieve optimal performance at masking rates of 60% and 40%, respectively, while Retail and Alibaba perform best with a 20% masking ratio. This difference may stem from the higher anomaly rates in YelpChi and Amazon, providing richer self-supervised signals for reconstructing masked node information. We can conclude that removing some unnecessary connections helps to anomalously reduce the amount of redundant information propagated from the normal majority.

3) *The effect of weights  $\alpha$  and  $\beta$  that balance the importance of attribute and structure reconstruction:* We conduct a sensitivity analysis of  $\alpha$  and  $\beta$ , which balance attribute and structure reconstructions in the original and augmented views. As shown in Fig. 5, the model's performance declines sharply for extreme values of  $\alpha$  and  $\beta$  ( $< 0.2$  or  $> 0.8$ ), highlighting the importance of maintaining a balance. The AUC first increases and then decreases as  $\alpha$  and  $\beta$  grow, with optimal performance of our proposed UMGAD at  $\alpha = 0.5, 0.5, 0.6, 0.5$  and  $\beta = 0.4, 0.4, 0.3, 0.3$  across the four datasets.

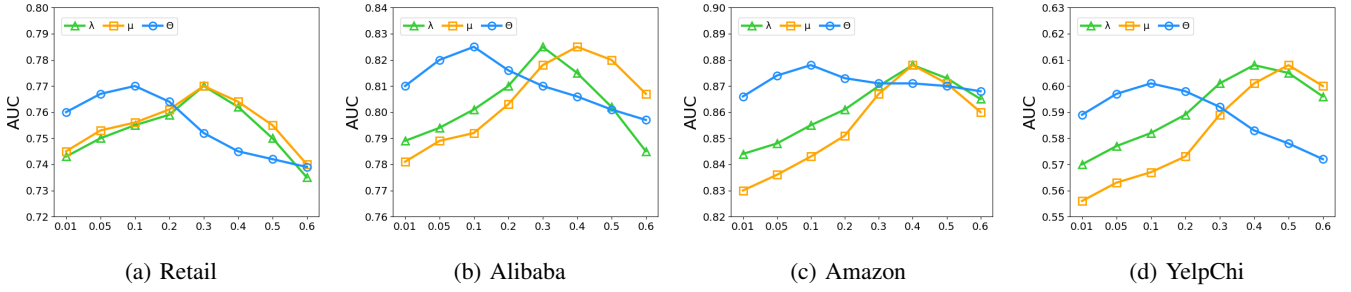


Fig. 3: The effect of hyperparameters  $\lambda$  and  $\mu$  in the final loss function.

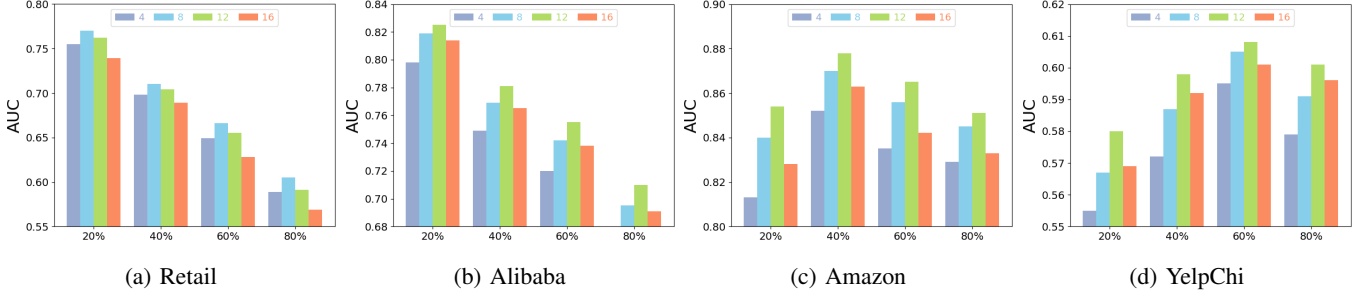


Fig. 4: The effect of masking ratio and masking subgraph size. The X-axis indicates the mask ratio, and 4 to 16 in the legend indicates the subgraph size.

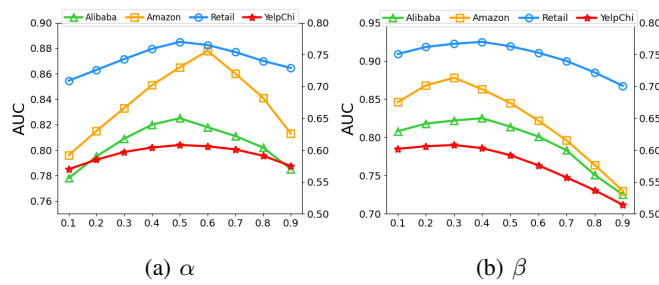


Fig. 5: The effect of weights  $\alpha$  and  $\beta$  in four datasets. The corresponding AUC values for the Alibaba and Amazon datasets are on the left Y-axis, and the corresponding AUC values for Retail and YelpChi are on the right Y-axis.

#### F. Performance Comparison in the Ground Truth Leakage Scenario (RQ5)

In this experiment, following [46], we determine the anomaly score thresholds for all methods on each dataset based on the number of anomalies. The experimental results are presented in Table IV. As shown in Table IV, even when ground truth information is incorporated, our model still achieves the best performance. This demonstrates that UMGAD effectively captures anomaly information and identifies anomalous nodes with greater accuracy compared to other methods.

For traditional GAD methods, Radar utilizes residual networks to learn node attributes and capture anomalies in a simple and effective manner. However, it struggles to capture anomalous features when dealing with complex network structures. Among specifically designed MPI methods, TAM outperforms ComGA and RAND by learning custom node

embeddings for anomaly detection. It maximizes the local affinity between nodes and their neighbors, while minimizing the influence of non-homogeneous edges linking abnormal and normal nodes.

CL-based GAD methods, such as GRADATE, VGOD, and ARISE, stand out as the most effective approaches. All three methods emphasize the importance of anomalous structural subgraphs in the GAD problem, leveraging subgraph sampling strategies to learn subgraph features and capture structural anomalies that are difficult for other methods to detect. In the realm of GAE-based GAD methods, most focus on improving the detection of anomalous nodes by learning better features during the reconstruction of attribute and structural information. The four most effective and representative methods in this category are GADAM, AnomMAN, GAD-NR, and ADA-GAD. ADA-GAD enhances anomalous node feature learning through graph augmentation, GAD-NR incorporates neighborhood reconstruction into the GAD task, and GADAM improves anomaly detection performance through enhanced GNN message passing. However, these methods fall short when addressing the GAD problem on multiplex heterogeneous graphs, leading to slightly lower performance compared to our UMGAD. AnomMAN distinguishes itself by targeting multiplex heterogeneous graphs constructed from ordinary heterogeneous graphs, which aligns with the focus of our UMGAD. However, its performance is limited due to its inability to effectively capture subgraph structural anomalies.

#### G. Model Efficiency Analysis (RQ6)

To evaluate the time efficiency of UMGAD, we compare its single-epoch and total runtime across four datasets against

TABLE IV: Performance comparison of all models on four datasets in the scenario of anomaly score threshold selection with ground truth leakage.

Method		Retail		Alibaba		Amazon		YelpChi	
		AUC	macro-F1	AUC	macro-F1	AUC	macro-F1	AUC	macro-F1
Trad.	Radar [IJCAI'17]	0.678 $\pm$ 0.003	0.570 $\pm$ 0.001	0.695 $\pm$ 0.011	0.621 $\pm$ 0.009	0.659 $\pm$ 0.003	0.564 $\pm$ 0.002	0.515 $\pm$ 0.003	0.502 $\pm$ 0.005
MPI	ComGA [WSDM'22]	0.702 $\pm$ 0.009	0.648 $\pm$ 0.003	0.761 $\pm$ 0.008	0.652 $\pm$ 0.002	0.715 $\pm$ 0.004	0.630 $\pm$ 0.007	0.543 $\pm$ 0.011	0.497 $\pm$ 0.006
	RAND [ICDM'23]	0.726 $\pm$ 0.006	0.678 $\pm$ 0.007	0.784 $\pm$ 0.008	0.677 $\pm$ 0.004	0.730 $\pm$ 0.013	0.645 $\pm$ 0.006	0.554 $\pm$ 0.007	0.504 $\pm$ 0.008
	TAM [NeurIPS'24]	0.753 $\pm$ 0.001	0.703 $\pm$ 0.001	0.795 $\pm$ 0.001	0.715 $\pm$ 0.001	0.840 $\pm$ 0.001	0.732 $\pm$ 0.001	0.582 $\pm$ 0.001	0.554 $\pm$ 0.001
CL	CoLA [TNNLS'21]	0.629 $\pm$ 0.009	0.559 $\pm$ 0.006	0.647 $\pm$ 0.014	0.613 $\pm$ 0.003	0.661 $\pm$ 0.006	0.579 $\pm$ 0.002	0.480 $\pm$ 0.005	0.489 $\pm$ 0.009
	ANEMONE [CIKM'21]	0.689 $\pm$ 0.004	0.631 $\pm$ 0.004	0.710 $\pm$ 0.007	0.632 $\pm$ 0.009	0.704 $\pm$ 0.002	0.614 $\pm$ 0.005	0.541 $\pm$ 0.005	0.511 $\pm$ 0.003
	Sub-CR [IJCAT'22]	0.704 $\pm$ 0.009	0.624 $\pm$ 0.008	0.728 $\pm$ 0.006	0.648 $\pm$ 0.008	0.675 $\pm$ 0.018	0.591 $\pm$ 0.003	0.520 $\pm$ 0.014	0.491 $\pm$ 0.008
	ARISE [TNNLS'23]	0.740 $\pm$ 0.018	0.683 $\pm$ 0.005	0.774 $\pm$ 0.006	0.669 $\pm$ 0.003	0.768 $\pm$ 0.006	0.679 $\pm$ 0.002	0.565 $\pm$ 0.001	0.525 $\pm$ 0.007
	SL-GAD [TKDE'21]	0.725 $\pm$ 0.003	0.667 $\pm$ 0.007	0.778 $\pm$ 0.005	0.672 $\pm$ 0.003	0.725 $\pm$ 0.009	0.642 $\pm$ 0.010	0.553 $\pm$ 0.011	0.504 $\pm$ 0.005
	PREM [ICDM'23]	0.724 $\pm$ 0.001	0.675 $\pm$ 0.003	0.782 $\pm$ 0.011	0.670 $\pm$ 0.009	0.735 $\pm$ 0.007	0.649 $\pm$ 0.006	0.557 $\pm$ 0.003	0.513 $\pm$ 0.007
	GCCAD [TKDE'22]	0.731 $\pm$ 0.003	0.677 $\pm$ 0.005	0.788 $\pm$ 0.002	0.689 $\pm$ 0.003	0.733 $\pm$ 0.001	0.647 $\pm$ 0.005	0.553 $\pm$ 0.002	0.516 $\pm$ 0.006
	GRADATE [AAAI'23]	0.746 $\pm$ 0.008	0.686 $\pm$ 0.005	0.790 $\pm$ 0.014	0.705 $\pm$ 0.013	0.805 $\pm$ 0.007	0.719 $\pm$ 0.005	0.574 $\pm$ 0.005	0.544 $\pm$ 0.006
	VGOD [ICDE'23]	0.745 $\pm$ 0.002	0.679 $\pm$ 0.003	0.791 $\pm$ 0.005	0.703 $\pm$ 0.003	0.797 $\pm$ 0.001	0.707 $\pm$ 0.006	0.571 $\pm$ 0.006	0.531 $\pm$ 0.008
GAE	DOMINANT [arXiv'16]	0.681 $\pm$ 0.013	0.625 $\pm$ 0.011	0.699 $\pm$ 0.019	0.625 $\pm$ 0.011	0.694 $\pm$ 0.007	0.605 $\pm$ 0.005	0.539 $\pm$ 0.003	0.509 $\pm$ 0.003
	GCNAE [SDM'19]	0.683 $\pm$ 0.005	0.633 $\pm$ 0.006	0.701 $\pm$ 0.017	0.631 $\pm$ 0.019	0.679 $\pm$ 0.010	0.591 $\pm$ 0.012	0.541 $\pm$ 0.009	0.511 $\pm$ 0.006
	AnomalyDAE [ICASSP'20]	0.679 $\pm$ 0.009	0.622 $\pm$ 0.004	0.697 $\pm$ 0.023	0.626 $\pm$ 0.018	0.708 $\pm$ 0.018	0.610 $\pm$ 0.024	0.545 $\pm$ 0.014	0.515 $\pm$ 0.007
	AdONE [WSDM'20]	0.685 $\pm$ 0.009	0.624 $\pm$ 0.004	0.707 $\pm$ 0.020	0.637 $\pm$ 0.018	0.721 $\pm$ 0.015	0.634 $\pm$ 0.014	0.556 $\pm$ 0.011	0.526 $\pm$ 0.018
	GAD-NR [WSDM'24]	0.749 $\pm$ 0.002	0.691 $\pm$ 0.003	0.789 $\pm$ 0.013	0.710 $\pm$ 0.015	0.829 $\pm$ 0.001	0.721 $\pm$ 0.006	0.579 $\pm$ 0.002	0.550 $\pm$ 0.008
	ADA-GAD [AAAI'24]	0.742 $\pm$ 0.009	0.702 $\pm$ 0.010	0.795 $\pm$ 0.003	0.716 $\pm$ 0.004	0.841 $\pm$ 0.016	0.732 $\pm$ 0.014	0.582 $\pm$ 0.003	0.549 $\pm$ 0.006
	GADAM [ICLR'24]	0.751 $\pm$ 0.001	0.702 $\pm$ 0.003	0.796 $\pm$ 0.009	0.713 $\pm$ 0.011	0.838 $\pm$ 0.003	0.728 $\pm$ 0.001	0.580 $\pm$ 0.005	0.554 $\pm$ 0.005
MV	AnomMAN [IS'23]	0.750 $\pm$ 0.008	0.703 $\pm$ 0.006	0.792 $\pm$ 0.006	0.714 $\pm$ 0.007	0.839 $\pm$ 0.007	0.728 $\pm$ 0.005	0.577 $\pm$ 0.011	0.552 $\pm$ 0.0010
	DualGAD [IS'23]	0.752 $\pm$ 0.005	0.700 $\pm$ 0.008	0.789 $\pm$ 0.013	0.714 $\pm$ 0.014	0.835 $\pm$ 0.008	0.727 $\pm$ 0.004	0.578 $\pm$ 0.006	0.550 $\pm$ 0.009
	<b>UMGAD</b>	<b>0.780<math>\pm</math>0.004</b>	<b>0.728<math>\pm</math>0.007</b>	<b>0.831<math>\pm</math>0.003</b>	<b>0.744<math>\pm</math>0.0006</b>	<b>0.886<math>\pm</math>0.004</b>	<b>0.793<math>\pm</math>0.002</b>	<b>0.612<math>\pm</math>0.002</b>	<b>0.600<math>\pm</math>0.004</b>
	<i>Improvement</i>	3.59% $\uparrow$	3.56% $\uparrow$	4.40% $\uparrow$	3.91% $\uparrow$	5.35% $\uparrow$	8.33% $\uparrow$	4.24% $\uparrow$	3.53% $\uparrow$

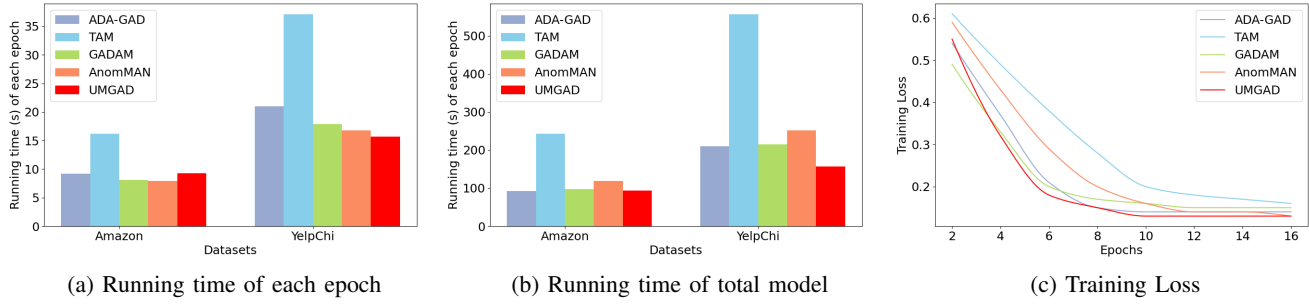


Fig. 6: Efficiency analysis of methods.

the four top-performing SOTA models: ADA-GAD, TAM, GADAM, and AnomMAN. As shown in Fig. 6, although UMGAD is not the fastest on the Amazon dataset in terms of single-epoch and total runtime, it remains highly competitive with these leading approaches. Significantly, on the YelpChi dataset, UMGAD achieves the shortest total runtime among all baselines, highlighting its superior efficiency. Additionally, as depicted in Fig. 6c, UMGAD demonstrates rapid convergence during training, reaching optimal performance with fewer epochs. This combination of efficiency and robust anomaly detection performance underscores UMGAD’s practicality and scalability, making it a probably choice for large-scale, time-sensitive graph analysis tasks.

## VI. CONCLUSION

In this work, we propose UMGAD, a novel framework tailored for UGAD tasks. To comprehensively capture diverse

anomaly signals, UMGAD employs a collaborative network that integrates graph autoencoders with diverse masking strategies across multiple relation types. These strategies operate effectively in both original and augmented views, enabling the model to extract meaningful patterns while filtering out redundant information. Leveraging attribute and structure reconstruction in the augmented view, followed by anomaly aggregation through dual-view contrastive learning, UMGAD achieves robust and adaptive detection. Extensive experiments on datasets with synthetic and real-world anomalies demonstrate that UMGAD outperforms state-of-the-art methods in unsupervised anomaly detection, excelling in both performance and efficiency. Ablation studies further validate the contribution of each component. In future work, we aim to explore simpler yet highly efficient models to push the boundaries of UGAD tasks.

## REFERENCES

[1] K. Ding, J. Li, N. Agarwal, and H. Liu, “Inductive anomaly detection on attributed networks,” in *Proceedings of the twenty-ninth international conference on international joint conferences on artificial intelligence*, 2021, pp. 1288–1294.

[2] X. Ma, J. Wu, S. Xue, J. Yang, C. Zhou, Q. Z. Sheng, H. Xiong, and L. Akoglu, “A comprehensive survey on graph anomaly detection with deep learning,” *IEEE Transactions on Knowledge and Data Engineering*, vol. 35, no. 12, pp. 12 012–12 038, 2021.

[3] Z. Chai, S. You, Y. Yang, S. Pu, J. Xu, H. Cai, and W. Jiang, “Can abnormality be detected by graph neural networks?” in *IJCAI*, 2022, pp. 1945–1951.

[4] X. Huang, Y. Yang, Y. Wang, C. Wang, Z. Zhang, J. Xu, L. Chen, and M. Vazirgiannis, “Dgraph: A large-scale financial dataset for graph anomaly detection,” *Advances in Neural Information Processing Systems*, vol. 35, pp. 22 765–22 777, 2022.

[5] Y. Dou, Z. Liu, L. Sun, Y. Deng, H. Peng, and P. S. Yu, “Enhancing graph neural network-based fraud detectors against camouflaged fraudsters,” in *Proceedings of the 29th ACM international conference on information & knowledge management*, 2020, pp. 315–324.

[6] C. Liu, L. Sun, X. Ao, J. Feng, Q. He, and H. Yang, “Intention-aware heterogeneous graph attention networks for fraud transactions detection,” in *Proceedings of the 27th ACM SIGKDD conference on knowledge discovery & data mining*, 2021, pp. 3280–3288.

[7] Y. Liu, X. Ao, Z. Qin, J. Chi, J. Feng, H. Yang, and Q. He, “Pick and choose: a gnn-based imbalanced learning approach for fraud detection,” in *Proceedings of the web conference 2021*, 2021, pp. 3168–3177.

[8] T. Chen and C. Tsourakakis, “Antibenford subgraphs: Unsupervised anomaly detection in financial networks,” in *Proceedings of the 28th ACM SIGKDD Conference on Knowledge Discovery and Data Mining*, 2022, pp. 2762–2770.

[9] Y. Yang, Y. Xu, Y. Sun, Y. Dong, F. Wu, and Y. Zhuang, “Mining fraudsters and fraudulent strategies in large-scale mobile social networks,” *IEEE Transactions on Knowledge and Data Engineering*, vol. 33, no. 1, pp. 169–179, 2019.

[10] L. Cheng, R. Guo, K. Shu, and H. Liu, “Causal understanding of fake news dissemination on social media,” in *Proceedings of the 27th ACM SIGKDD Conference on Knowledge Discovery & Data Mining*, 2021, pp. 148–157.

[11] E. Min, Y. Rong, Y. Bian, T. Xu, P. Zhao, J. Huang, and S. Ananiadou, “Divide-and-conquer: Post-user interaction network for fake news detection on social media,” in *Proceedings of the ACM web conference 2022*, 2022, pp. 1148–1158.

[12] Y. Cao, H. Peng, Z. Yu, and S. Y. Philip, “Hierarchical and incremental structural entropy minimization for unsupervised social event detection,” in *Proceedings of the AAAI Conference on Artificial Intelligence*, vol. 38, no. 8, 2024, pp. 8255–8264.

[13] H. Tang, X. Liang, J. Wang, and S. Zhang, “Dualgad: Dual-bootstrapped self-supervised learning for graph anomaly detection,” *Information Sciences*, vol. 668, p. 120520, 2024.

[14] Z. Gong, G. Wang, Y. Sun, Q. Liu, Y. Ning, H. Xiong, and J. Peng, “Beyond homophily: Robust graph anomaly detection via neural sparsification,” in *IJCAI*, 2023, pp. 2104–2113.

[15] J. Zhang, Z. Xu, D. Lv, Z. Shi, D. Shen, J. Jin, and F. Dong, “Digin-gnn: Discriminative feature guided gnn-based fraud detector against inconsistencies in multi-relation fraud graph,” in *Proceedings of the AAAI Conference on Artificial Intelligence*, vol. 38, no. 8, 2024, pp. 9323–9331.

[16] S. Yang, B. Zhang, S. Feng, Z. Tan, Q. Zheng, J. Zhou, and M. Luo, “Ahead: A triple attention based heterogeneous graph anomaly detection approach,” in *Chinese Intelligent Automation Conference*. Springer, 2023, pp. 542–552.

[17] Y. Gao, X. Wang, X. He, Z. Liu, H. Feng, and Y. Zhang, “Addressing heterophily in graph anomaly detection: A perspective of graph spectrum,” in *Proceedings of the ACM Web Conference 2023*, 2023, pp. 1528–1538.

[18] F. Xu, N. Wang, H. Wu, X. Wen, X. Zhao, and H. Wan, “Revisiting graph-based fraud detection in sight of heterophily and spectrum,” in *Proceedings of the AAAI Conference on Artificial Intelligence*, vol. 38, no. 8, 2024, pp. 9214–9222.

[19] G. Zhang, Z. Yang, J. Wu, J. Yang, S. Xue, H. Peng, J. Su, C. Zhou, Q. Z. Sheng, L. Akoglu *et al.*, “Dual-discriminative graph neural network for imbalanced graph-level anomaly detection,” *Advances in Neural Information Processing Systems*, vol. 35, pp. 24 144–24 157, 2022.

[20] J. Tang, J. Li, Z. Gao, and J. Li, “Rethinking graph neural networks for anomaly detection,” in *International Conference on Machine Learning*. PMLR, 2022, pp. 21 076–21 089.

[21] S. Zhou, X. Huang, N. Liu, H. Zhou, F.-L. Chung, and L.-K. Huang, “Improving generalizability of graph anomaly detection models via data augmentation,” *IEEE Transactions on Knowledge and Data Engineering*, vol. 35, no. 12, pp. 12 721–12 735, 2023.

[22] F. Liu, X. Ma, J. Wu, J. Yang, S. Xue, A. Beheshti, C. Zhou, H. Peng, Q. Z. Sheng, and C. C. Aggarwal, “Dagad: Data augmentation for graph anomaly detection,” in *2022 IEEE international conference on data mining (ICDM)*. IEEE, 2022, pp. 259–268.

[23] Z. Xie, H. Xu, W. Chen, W. Li, H. Jiang, L. Su, H. Wang, and D. Pei, “Unsupervised anomaly detection on microservice traces through graph vae,” in *Proceedings of the ACM Web Conference 2023*, 2023, pp. 2874–2884.

[24] B. Xu, J. Wang, Z. Zhao, H. Lin, and F. Xia, “Unsupervised anomaly detection on attributed networks with graph contrastive learning for consumer electronics security,” *IEEE Transactions on Consumer Electronics*, 2024.

[25] F. Zhang, S. Kan, D. Zhang, Y. Cen, L. Zhang, and V. Mladenovic, “A graph model-based multiscale feature fitting method for unsupervised anomaly detection,” *Pattern Recognition*, vol. 138, p. 109373, 2023.

[26] N. Wang, Z. Wang, Y. Gong, Z. Huang, Z. Huang, X. Wen, and H. Zeng, “Unsupervised data anomaly detection based on graph neural network,” in *The International Conference on Cyber Security Intelligence and Analytics*. Springer, 2023, pp. 552–564.

[27] J. Li, H. Dani, X. Hu, and H. Liu, “Radar: Residual analysis for anomaly detection in attributed networks,” in *IJCAI*, vol. 17, 2017, pp. 2152–2158.

[28] X. Luo, J. Wu, A. Beheshti, J. Yang, X. Zhang, Y. Wang, and S. Xue, “Comga: Community-aware attributed graph anomaly detection,” in *Proceedings of the Fifteenth ACM International Conference on Web Search and Data Mining*, 2022, pp. 657–665.

[29] H. Qiao and G. Pang, “Truncated affinity maximization: One-class homophily modeling for graph anomaly detection,” *Advances in Neural Information Processing Systems*, vol. 36, 2024.

[30] B. Chen, J. Zhang, X. Zhang, Y. Dong, J. Song, P. Zhang, K. Xu, E. Kharlamov, and J. Tang, “Gecad: Graph contrastive coding for anomaly detection,” *IEEE Transactions on Knowledge and Data Engineering*, vol. 35, no. 8, pp. 8037–8051, 2022.

[31] J. Duan, S. Wang, P. Zhang, E. Zhu, J. Hu, H. Jin, Y. Liu, and Z. Dong, “Graph anomaly detection via multi-scale contrastive learning networks with augmented view,” in *Proceedings of the AAAI conference on artificial intelligence*, vol. 37, no. 6, 2023, pp. 7459–7467.

[32] Y. Huang, L. Wang, F. Zhang, and X. Lin, “Unsupervised graph outlier detection: Problem revisit, new insight, and superior method,” in *2023 IEEE 39th International Conference on Data Engineering (ICDE)*. IEEE, 2023, pp. 2565–2578.

[33] J. He, Q. Xu, Y. Jiang, Z. Wang, and Q. Huang, “Ada-gad: Anomaly-denoised autoencoders for graph anomaly detection,” in *Proceedings of the AAAI Conference on Artificial Intelligence*, vol. 38, no. 8, 2024, pp. 8481–8489.

[34] Y. Pei, T. Huang, W. van Ipenburg, and M. Pechenizkiy, “Resgc: attention-based deep residual modeling for anomaly detection on attributed networks,” *Machine Learning*, vol. 111, no. 2, pp. 519–541, 2022.

[35] L. Wang, P. Li, K. Xiong, J. Zhao, and R. Lin, “Modeling heterogeneous graph network on fraud detection: A community-based framework with attention mechanism,” in *Proceedings of the 30th ACM international conference on information & knowledge management*, 2021, pp. 1959–1968.

[36] Y. Bei, S. Zhou, Q. Tan, H. Xu, H. Chen, Z. Li, and J. Bu, “Reinforcement neighborhood selection for unsupervised graph anomaly detection,” in *2023 IEEE International Conference on Data Mining (ICDM)*. IEEE, 2023, pp. 11–20.

[37] Y. Liu, K. Ding, Q. Lu, F. Li, L. Y. Zhang, and S. Pan, “Towards self-interpretable graph-level anomaly detection,” *Advances in Neural Information Processing Systems*, vol. 36, 2024.

[38] X. Kong, W. Zhang, H. Wang, M. Hou, X. Chen, X. Yan, and S. K. Das, “Federated graph anomaly detection via contrastive self-supervised learning,” *IEEE Transactions on Neural Networks and Learning Systems*, 2024.

[39] J. Liu, M. He, X. Shang, J. Shi, B. Cui, and H. Yin, “Bourne: Bootstrapped self-supervised learning framework for unified graph anomaly detection,” in *2024 IEEE 40th International Conference on Data Engineering (ICDE)*. IEEE, 2024, pp. 2820–2833.

[40] Q. Wang, G. Pang, M. Salehi, W. Buntine, and C. Leckie, “Cross-domain graph anomaly detection via anomaly-aware contrastive alignment,” in *Proceedings of the AAAI Conference on Artificial Intelligence*, vol. 37, no. 4, 2023, pp. 4676–4684.

[41] Y. Liu, Z. Li, S. Pan, C. Gong, C. Zhou, and G. Karypis, “Anomaly detection on attributed networks via contrastive self-supervised learning,” *IEEE transactions on neural networks and learning systems*, vol. 33, no. 6, pp. 2378–2392, 2021.

[42] J. Zhang, S. Wang, and S. Chen, “Reconstruction enhanced multi-view contrastive learning for anomaly detection on attributed networks,” *arXiv preprint arXiv:2205.04816*, 2022.

[43] Y. Li, X. Huang, J. Li, M. Du, and N. Zou, “Specae: Spectral autoencoder for anomaly detection in attributed networks,” in *Proceedings of the 28th ACM international conference on information and knowledge management*, 2019, pp. 2233–2236.

[44] K. Ding, J. Li, R. Bhanushali, and H. Liu, “Deep anomaly detection on attributed networks,” in *Proceedings of the 2019 SIAM international conference on data mining*. SIAM, 2019, pp. 594–602.

[45] A. Roy, J. Shu, J. Li, C. Yang, O. Elshocht, J. Smeets, and P. Li, “Gad-nr: Graph anomaly detection via neighborhood reconstruction,” in *Proceedings of the 17th ACM International Conference on Web Search and Data Mining*, 2024, pp. 576–585.

[46] L.-H. Chen, H. Li, W. Zhang, J. Huang, X. Ma, J. Cui, N. Li, and J. Yoo, “Anomman: Detect anomalies on multi-view attributed networks,” *Information Sciences*, vol. 628, pp. 1–21, 2023.

[47] X. Ren, L. Xia, Y. Yang, W. Wei, T. Wang, X. Cai, and C. Huang, “Sslrec: A self-supervised learning framework for recommendation,” in *Proceedings of the 17th ACM International Conference on Web Search and Data Mining*, 2024, pp. 567–575.

[48] C. Fu, G. Zheng, C. Huang, Y. Yu, and J. Dong, “Multiplex heterogeneous graph neural network with behavior pattern modeling,” in *Proceedings of the 29th ACM SIGKDD Conference on Knowledge Discovery and Data Mining*, 2023, pp. 482–494.

[49] S. Kumar, X. Zhang, and J. Leskovec, “Predicting dynamic embedding trajectory in temporal interaction networks,” in *Proceedings of the 25th ACM SIGKDD international conference on knowledge discovery & data mining*, 2019, pp. 1269–1278.

[50] M. Jin, Y. Liu, Y. Zheng, L. Chi, Y.-F. Li, and S. Pan, “Anemone: Graph anomaly detection with multi-scale contrastive learning,” in *Proceedings of the 30th ACM international conference on information & knowledge management*, 2021, pp. 3122–3126.

[51] J. Duan, B. Xiao, S. Wang, H. Zhou, and X. Liu, “Arise: Graph anomaly detection on attributed networks via substructure awareness,” *IEEE transactions on neural networks and learning systems*, 2023.

[52] Y. Zheng, M. Jin, Y. Liu, L. Chi, K. T. Phan, and Y.-P. P. Chen, “Generative and contrastive self-supervised learning for graph anomaly detection,” *IEEE Transactions on Knowledge and Data Engineering*, vol. 35, no. 12, pp. 12220–12233, 2021.

[53] J. Pan, Y. Liu, Y. Zheng, and S. Pan, “Prem: A simple yet effective approach for node-level graph anomaly detection,” in *2023 IEEE International Conference on Data Mining (ICDM)*. IEEE, 2023, pp. 1253–1258.

[54] T. N. Kipf and M. Welling, “Variational graph auto-encoders,” *arXiv preprint arXiv:1611.07308*, 2016.

[55] H. Fan, F. Zhang, and Z. Li, “Anomalydae: Dual autoencoder for anomaly detection on attributed networks,” in *ICASSP 2020-2020 IEEE International Conference on Acoustics, Speech and Signal Processing (ICASSP)*. IEEE, 2020, pp. 5685–5689.

[56] S. Bandyopadhyay, L. N. S. V. Vivek, and M. N. Murty, “Outlier resistant unsupervised deep architectures for attributed network embedding,” in *Proceedings of the 13th international conference on web search and data mining*, 2020, pp. 25–33.

[57] J. Chen, G. Zhu, C. Yuan, and Y. Huang, “Boosting graph anomaly detection with adaptive message passing,” in *The Twelfth International Conference on Learning Representations*, 2024.